Metal–Organic Frameworks

DOI: 10.1002/anie.201007583

A Metal–Organic Framework with Optimized Open Metal Sites and Pore Spaces for High Methane Storage at Room Temperature**

Zhiyong Guo, Hui Wu, Gadipelli Srinivas, Yaming Zhou, Shengchang Xiang, Zhenxia Chen, Yongtai Yang, Wei Zhou, Michael O'Keeffe, and Banglin Chen**

Realization of high-capacity gas storage materials is essential to make use of clean energy resouces such as hydrogen, methane (natural gas), and acetylene in the future. Although there has been extensive research on gas storage materials, no feasible hydrogen storage materials have been achieved to date that meet the storage capacity needed at room temperature and moderate pressure, while the explosive nature of acetylene has excluded it as top priority; thus methane (natural gas) is considered to be the most promising alternative energy source, especially for mobile applications.[1] In fact, a MOF (metal–organic framework) methane fuel tank has already been implemented in test vehicles.[2]

Highly porous MOFs with large pore space and high surface areas apparently favor high gas storage capacities; however, the relatively weak interactions with gas molecules have limited their high gas storage capacities to low temperature (for example, 77 K for H_2) or high pressure (up to 100 bar) to fully utilize the pore space.[3–11] Furthermore, the low framework densities of some extremely porous MOFs have also limited their volumetric gas storage capacities, another important parameter for the practical implementation of such materials in mobile applications. Accordingly, the ideal MOF materials for high volumetric gas storage are those with moderate porosities in which the pore spaces and functional sites are efficiently utilized through strong interactions with gas molecules; thus their storage capacities can be maximized at room temperature and lower pressures of 35 bar. Our design principle to maximize high-density methane storage is to 1) immobilize high-density open metal sites and to 2) construct suitable pore spaces within a metal–organic framework. We report herein its implementation in $[Cu_3(BHB)]$ (which we term UTSA-20; UTSA = University of Texas at San Antonio) with a structure based on the novel trinodal (3,3,4) net of **zyg** topology (Figure 1c),[12] which is formed by the self-assembly of a hexacarboxylate organic linker H_6BHB (H_6BHB = 3,3′,3″,5,5′,5″-benzene-1,3,5-triyl-hexabenzoic acid, Figure 1a) with the paddle-wheel $Cu_2(COO)_4$ SBU (Figure 1b).[13] The density of open copper sites has been secured by the six carboxylates, while the pore spaces have been optimized by the *m*-benzenedicarboxylate moieties and the central benzene backbone. The high density of open copper sites and optimal pore spaces within UTSA-20 has enabled them to be fully utilized for methane storage, highlighting UTSA-20 as the material with the highest methane storage density (0.222 g cm^{-3}) in micropores at 300 K and 35 bar. The overall absolute volumetric methane storage of 195 cm^3 cm^{-3} has resulted in UTSA-20 being one of the very few MOFs surpassing the DOE methane storage target of 180 cm^3 cm^{-3} at room temperature and 35 bar.[14]

UTSA-20 was synthesized by the solvothermal reaction of H_6BHB (10 mg, 0.018 mmol) and $Cu(NO_3)_2{\cdot}2.5H_2O$ (20 mg, 0.086 mmol) in *N,N*-dimethylformamide (DMF, 1.5 mL) with addition of two drops of HBF_4 at 65 °C for 48 hours to give small green block-shaped crystals (15.8 mg, 69% yield based on H_6BHB). The compound was formulated as $[Cu_3(BHB)(H_2O)_3]{\cdot}(DMF)_6(H_2O)_{2.5}$ on the basis of elemental microanalysis.[15]

Acetone-exchanged UTSA-20 was activated at 120 °C for 24 hours under high vacuum for powder X-ray diffraction and gas sorption studies. As shown in Figure S1 in the Supporting Information, the activated UTSA-20 exhibits a well-resolved PXRD pattern, which has allowed us to refine the structure by powder X-ray Rietveld refinement.

As expected, the paddle-wheel $Cu_2(CO_2)_4$ SBUs formed in situ are bridged by the hexadentate organic BHB linkers to construct a three-dimensional porous MOF based on a novel trinodal (3,3,4)-coordinated net of **zyg** topology, consisting of two kinds of three-coordinated nodes, shown as blue and green triangles, and a four-coordinated node of the paddle-wheel $Cu_2(CO_2)_4$ cluster, shown as a red square (Figure 1). The **zyg** net is significantly different from the **ntt** one

[*] Dr. Z. Guo, Dr. S. Xiang, Prof. Dr. B. Chen
Department of Chemistry, University of Texas at San Antonio
One UTSA Circle, San Antonio, Texas 78249-0698 (USA)
Fax: (+1) 210-458-7428
E-mail: banglin.chen@utsa.edu
Homepage: http://www.utsa.edu/chem/chen.html
Dr. H. Wu, Dr. W. Zhou
NIST Center for Neutron Research
Gaithersburg, Maryland 20899-6102 (USA)
and
Department of Materials Science and Engineering
University of Maryland, College Park, Maryland 20742 (USA)
E-mail: wzhou@nist.gov
Dr. G. Srinivas
NIST Center for Neutron Research, Gaithersburg (USA)
and
Department of Materials Science and Engineering
University of Pennsylvania (USA)
Prof. Dr. Y. Zhou, Dr. Z. Chen, Y. Yang
Department of Chemistry, Fudan University (China)
Prof. Dr. M. O'Keeffe
Department of Chemistry and Biochemistry
Arizona State University (USA)

[**] This work was supported by the award CHE 0718281 from the NSF and AX-1730 from the Welch Foundation (B.C.).

Supporting information for this article is available on the WWW under http://dx.doi.org/10.1002/anie.201007583.

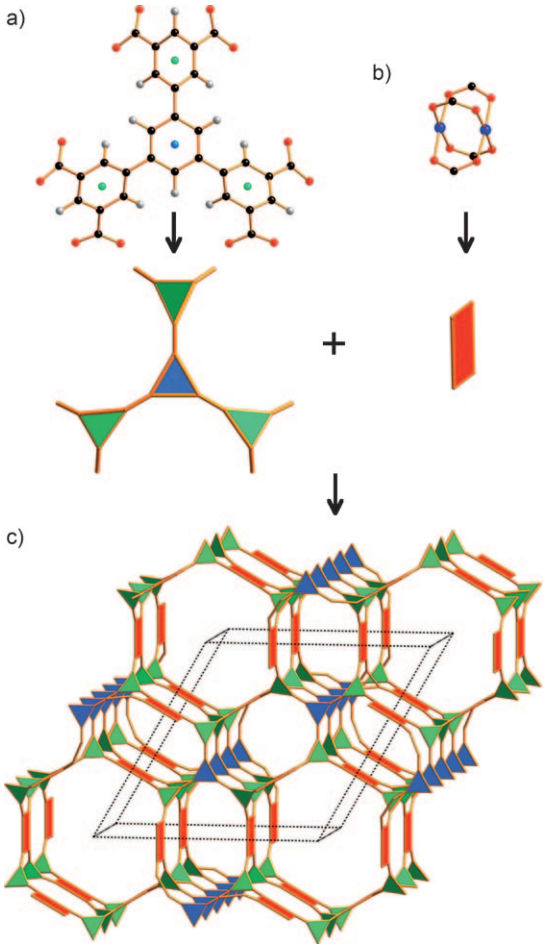

Figure 1. a, b) The secondary building units (SBUs) of UTSA-20 (C black, O red, Cu blue). The isolated blue and green points on the BHB linker indicate the branching points (nodes) of the underlying **zyg** net. In the middle, the SBUs are shown abstracted as geometric shapes. c) The assembly of these shapes in UTSA-20. The topology is **zyg-a** (the augmented **zyg** net in which coordination figures (in this case squares and triangles) replace the original vertices).

constructed from the $Cu_2(CO_2)_4$ clusters and larger hexadentate organic linkers, mainly because the four benzene rings within BHB are tilted with respect to each other and are not coplanar owing to the constraints of the crystal structure (Figures S2 and S3 in the Supporting Information).[5–8] There are 1D rectangular pores of about 3.4 × 4.8 Å and 1D cylinders of 8.5 Å in diameter along the *c* axis, taking into account the van der Waals radii, with the open copper sites exposed to the pores for the potential binding and storage of gas molecules. The total accessible free volume is 3471.0 $Å^3$, or 63.0% of the unit volume 5512.9 $Å^3$.

As shown in Figure 2a, UTSA-20 exhibits type I reversible sorption isotherms and takes up N_2 to 402 $cm^3 g^{-1}$ at 77 K and 1 bar, corresponding to a BET surface area of 1156 $m^2 g^{-1}$.[16] Such porosity is moderate and is even lower than those of HKUST-1 ($[Cu_2(BTC)_3]$, BTC = 1,3,5-benzenetricarboxylate) and MOF-505 ($[Cu_2(BPTC)]$, BPTC = 3,3′,5,5′-biphenyltetracarboxylate).[17] However, the high density of open copper sites and small pores is favorable to the high hydrogen storage of 2.9 wt% at 77 K and 1 bar (Figure S4 in the Supporting Information), but the moderate surface area has apparently limited its hydrogen uptake to 4.1 wt% at 77 K and 15 bar (Figure S5 in the Supporting Information). Although both N_2 and H_2 sorption isotherms indicate that UTSA-20 is of moderate porosity, it takes up a significant amount of methane because of the full use of both open copper sites and optimal pore spaces for methane storage. The methane storage density at 150 K and 5 bar is 0.376 $g cm^{-3}$, which is 89% of that of liquid methane (0.423 $g cm^{-3}$). The methane storage density in micropores in UTSA-20 is 0.222 $g cm^{-3}$ at 300 K and 35 bar, which is almost the same as the density of compressed methane at 300 K and 340 bar, highlighting UTSA-20 as the porous material with the highest methane storage density at 300 K and 35 bar (storage density in micropores is the amount of methane stored divided by the volume of pore space).[18–27] A comparison of UTSA-20 and some reported MOFs for methane storage is shown in Table 1. The efficient use of the pore spaces contributes to the high excess volumetric methane storage capacity of UTSA-20 of 178 $cm^3 cm^{-3}$ at 300 K and 35 bar (Figure 2), which is slightly lower than the two best MOFs for volumetric methane storage (ca. 190 $cm^3 cm^{-3}$).[28] The overall absolute volumetric methane storage capacity is 195 $cm^3 cm^{-3}$, which surpasses the DOE standard (180 $cm^3 cm^{-3}$) of porous materials for methane storage at ambient temperature and 35 bar (Figure S6 in the Supporting Information).

The open copper sites and optimal pore spaces have also enabled high excess volumetric carbon dioxide storage in UTSA-20 (301 $cm^3 cm^{-3}$), which is comparable to those of highly porous MOFs with much larger surfaces areas (MIL-101 (5900 $m^2 g^{-1}$), 300 $cm^3 cm^{-3}$; MOF-177 (5640 $m^2 g^{-1}$), 323 $cm^3 cm^{-3}$; Figure S7 and Table S1 in the Supporting Information).[29]

The coverage-dependent adsorption enthalpies of methane to UTSA-20 were calculated based on the virial method,[17] a well-established and reliable methodology, from fits of the adsorption isotherms at 200, 240, 270, and 300 K. As shown in Figure S8 in the Supporting Information, UTSA-20 exhibits quite high adsorption enthalpies for CH_4

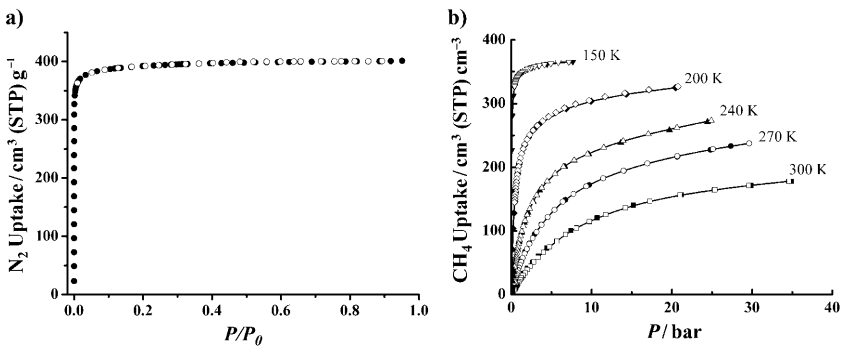

Figure 2. a) Nitrogen sorption isotherm at 77 K and b) variable-temperature high-pressure excess methane sorption isotherms of UTSA-20.

Table 1: Comparison of UTSA-20 with some previously reported MOFs for their methane storage at 298–300 K and 35 bar.

MOF	Surface area [$m^2 g^{-1}$]	Pore volume [$cm^3 g^{-1}$]	CH_4 uptake [cm^3(STP)cm^{-3}]	Density of adsorbed CH_4 [g^{cm-3}][b]
UTSA-20	1156	0.63	178	0.22
PCN-14[21]	1753	0.87	220[a]	0.21
Ni-MOF-74[26]	1033	0.54	190	0.21
IRMOF-6[20]	2800	0.92	155	0.19
$[CuSiF_6(4,4'\text{-bipy})_2]$[18]	1337	0.56	125	0.19
PCN-11[23]	1931	0.91	171	0.18
$[Zn_2(bdc)_2(dabco)]$[25]	1450	0.68	137	0.17
HKUST-1[27]	1502	0.76	160	0.17
IRMOF-1[20]	3800	1.04	135	0.15
MIL-101c[22]	4230	2.15	100	0.08
MOF-205[4]	4460	2.16	93	0.08
MOF-200[4]	4530	3.59	41	0.04
MOF-210[4]	6240	3.60	53	0.04

[a] At 290 K. [b] In micropores.

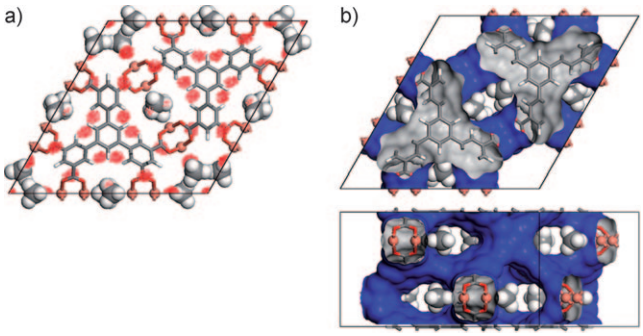

Figure 3. a) Probability distribution of the CH_4 center of mass in UTSA-20 ([001] view), obtained from GCMC simulation at 298 K and 10 bar. The red regions represent the places where methane molecules are heavily populated in the MOF structure. Note that the open Cu site is preoccupied with CH_4 molecules to focus our effort on the search for other strong methane adsorption sites. b) The pore surface of the interconnected channel pores in UTSA-20 (derived using N_2 as probe molecules, based on vdW interactions), with adsorbed methane at the linker channel site (derived from DFT-D calculations). The channel width along the *c* axis matches well with the size of the adsorbed methane molecules, leading to enhanced vdW interaction (methane molecules are shown in space-filling representation for clarity).

(17.7 kJ mol^{-1} at zero coverage), which are slightly higher than those for other MOFs that exhibit high-density methane storage.[26]

To investigate the methane adsorption and storage mechanism in UTSA-20, we performed detailed computational investigations. Previous studies on methane storage in other MOFs with dicopper paddle wheel units have well established that the open copper site binds CH_4 strongly and is one of the primary methane adsorption sites.[30] The same is expected for UTSA-20 since it contains the same open copper units. We note that direct binding of one methane molecule at each Cu site only accounts for a maximum storage capacity of approximately 89 cm^3(STP)cm^{-3}, half of the 178 cm^3(STP)cm^{-3} measured at room temperature and 35 bar. To reveal other major CH_4 adsorption sites, we performed grand canonical Monte Carlo (GCMC) simulations of methane adsorption in UTSA-20 (with the open Cu sites preoccupied by methane) using the classical force-field method.[31] Simulations were performed at 298 K and various pressures (0.1, 1, 10, and 35 bar). The probability distribution of adsorbed CH_4 was generated from the simulation after the equilibrium stage, and the result obtained at 10 bar is shown in Figure 3a as an example. Clearly, the channel-like pore spaces between the parallel stacks of BHB linkers (along the *c* axis) are heavily populated by CH_4 molecules, and we term this site the "linker channel site". At higher pressure, additional adsorption sites can be found, but they are much weaker and less well defined. We note that full saturation of the open copper site and the linker channel site can generate a methane capacity of about 162 cm^3(STP)cm^{-3}, which is approximately 90% of the experimental uptake at 298 K and 35 bar. The remaining storage capacity can be easily provided by those additional secondary adsorption sites.

We further explored the energy aspect of adsorption of methane on the two major sites. The static methane binding energies (E_B) were calculated based on density functional theory[32] with a semiempirical correction[33] for dispersive interactions (DFT-D). For the open Cu site and the linker channel site, calculated E_B values are 21.6 and 23.5 kJ mol^{-1}, respectively, in reasonable agreement with the above experimental Q_{st} values. Interestingly, the methane binding at the linker channel site is even stronger than that at the open Cu site. While the methane binding on the open Cu site was known to be partly due to the enhanced electrostatic interaction between the metal ion and the slightly polarized methane molecule, the methane interaction with the framework at the linker channel site is mainly of van der Waals (vdW) nature. We found that the size of the linker channel pore is just right to enable the methane molecule to interact with two BHB linkers simultaneously. To further illustrate this fit, in Figure 3b we plot the vdW surface of the UTSA-20 channel pores along with the adsorbed methane at the linker channel sites. Clearly, the methane molecule is "sandwiched" between two BHB linker potential surfaces, which results in enhanced overall interaction. The strong interactions of the both open copper sites and the linker channel sites with methane gas molecules have enabled the pore spaces within UTSA-20 to be fully utilized for methane storage, thus featuring UTSA-20 as the porous MOF with the highest methane storage density (Figure S9 in the Supporting Information).

In summary, we realized a 3D porous metal–organic framework (UTSA-20) based on a novel trinodal (3,3,4) net of **zyg** topology by the self-assembly of the nonlinear hexacarboxylate (BHB) with the paddle-wheel $Cu_2(COO)_4$ cluster. Although its porosity and surface area are moderate and much lower than those of most highly porous MOFs, the open copper sites and optimal pore spaces within UTSA-20 have enabled the pore spaces to be fully utilized for methane storage, featuring UTSA-20 as the material with the highest methane storage density (0.222 gcm^{-3}), and just the third porous MOF whose absolute volumetric methane storage has surpassed the DOE methane storage target of 180 $cm^3 cm^{-3}$ at room temperature and 35 bar. By the immobilization of a high density of open metal sites and the deliberate control of the

pore space for their efficient methane storage, these new porous MOFs are envisioned to be very promising media for methane and natural gas storage, particularly for mobile applications.

Experimental Section

In the powder X-ray crystallography investigation, phase identification was conducted on samples sealed in glass capillaries using a Rigaku X-ray diffractometer with a Cu K_α source. Data were collected over 14 h at room temperature in the 2θ range of 5–60° with a step size of 0.02°. The X-ray diffraction (XRD) reflections of the as-synthesized UTSA-20 samples can be indexed using a hexagonal cell with $a = 21.971$ and $c = 13.547$ Å. Evaluation of the systematic absences in the XRD pattern indicated the following most probable space groups: $P\bar{6}cm$, $P\bar{6}c2$, $P6_3/mcm$, $P31c$, and $P\bar{3}c1$. After activation, the symmetry of the UTSA-20 structure remains unchanged. We then solved the crystal structure using the direct method, and the space group was identified as $P6_3/mcm$. Finally, Rietveld refinement was performed on the XRD pattern collected on the activated sample, using the GSAS package.[34] Refinement on the lattice parameters, background, peak profile, as well as the atomic positions of Cu, C, and O with constraints applied on C–C and C–O bonds lengths yielded the agreement factors of $R_{wp} = 0.0811$ and $R_p = 0.0644$, which strongly supports the validity of our structure solution. Note that the quality and insensitivity of laboratory XRD data do not allow accurate location of H atoms, and thus the positions of H atoms were estimated from the geometry and the common length of CH bonds. The refined lattice parameters are $a = 22.286(1)$ and $c = 12.816(1)$ Å. CCDC-795055 (UTSA-20) contains the supplementary crystallographic data for this paper. These data can be obtained free of charge from The Cambridge Crystallographic Data Centre via www.ccdc.cam.ac.uk/data_request/cif.

Received: December 2, 2010
Revised: January 5, 2011
Published online: March 4, 2011

Keywords: methane storage · microporous materials · molecular recognition · open metal sites · organic-inorganic hybrid composites

[1] A. U. Czaja, N. Trukhan, U. Müller, *Chem. Soc. Rev.* **2009**, *38*, 1284.
[2] http://www.ecofuel-world-tour.com.
[3] a) O. M. Yaghi, M. O'Keeffe, N. W. Ockwig, H. K. Chae, M. Eddaoudi, J. Kim, *Nature* **2003**, *423*, 705; b) S. Kitagawa, R. Kitaura, S. Noro, *Angew. Chem.* **2004**, *116*, 2388; *Angew. Chem. Int. Ed.* **2004**, *43*, 2334; M. Dinca, J. R. Long, *Angew. Chem.* **2008**, *120*, 6870; *Angew. Chem. Int. Ed.* **2008**, *47*, 6766; c) R. E. Morris, P. S. Wheatley, *Angew. Chem.* **2008**, *120*, 5044; *Angew. Chem. Int. Ed.* **2008**, *47*, 4966; d) J. M. Thomas, *Top. Catal.* **2008**, *50*, 98; e) T. Dueren, Y.-S. Bae, R. Q. Snurr, *Chem. Soc. Rev.* **2009**, *38*, 1237; f) L. Ma, C. Abney, W. Lin, *Chem. Soc. Rev.* **2009**, *38*, 1248; g) G. Férey, C. Serre, *Chem. Soc. Rev.* **2009**, *38*, 1380; h) B. Chen, S.-C. Xiang, G.-D. Qian, *Acc. Chem. Res.* **2010**, *43*, 1115.
[4] H. Furukawa, N. Ko, Y. B. Go, N. Aratani, S. B. Choi, E. Choi, A. O. Yazaydin, R. Q. Snurr, M. O'Keeffe, J. Kim, O. M. Yaghi, *Science* **2010**, *239*, 424.
[5] O. K. Farha, A. O. Yazaydın, I. Eryazici, C. D. Malliakas, B. G. Hauser, M. G. Kanatzidis, S. T. Nguyen, R. Q. Snurr, J. T. Hupp, *Nat. Chem.* **2010**, *2*, 944.
[6] F. Nouar, J. F. Eubank, T. Bousquet, L. Wojtas, M. J. Zawarotko, M. Eddaoudi, *J. Am. Chem. Soc.* **2008**, *130*, 1833.
[7] D. Yuan, D. Zhao, D. Sun, H.-C. Zhou, *Angew. Chem.* **2010**, *122*, 5485; *Angew. Chem. Int. Ed.* **2010**, *49*, 5357.
[8] Y. Yan, I. Telepeni, S. Yang, X. Lin, W. Kockelmann, A. Dailly, A. J. Blake, W. Lewis, G. S. Walker, D. R. Allan, S. A. Barnett, N. R. Champness, M. Schroder, *J. Am. Chem. Soc.* **2010**, *132*, 4092.
[9] J. Zhang, T. Wu, S.- M. Chen, P. Feng, X. Bu, *Angew. Chem.* **2009**, *121*, 3538; *Angew. Chem. Int. Ed.* **2009**, *48*, 3486.
[10] Y.-B. Zhang, W.-X. Zhang, F.-Y. Feng, J.-P. Zhang, X.- M. Chen, *Angew. Chem.* **2009**, *121*, 5391; *Angew. Chem. Int. Ed.* **2009**, *48*, 5287.
[11] A. J. Lan, K. H. Li, H. H. Wu, D. H. Olson, T. J. Emge, W. Ki, M. C. Hong, J. Li, *Angew. Chem.* **2009**, *121*, 2370; *Angew. Chem. Int. Ed.* **2009**, *48*, 2334.
[12] M. O'Keeffe, M. A. Peskov. S. J. Ramsden, O. M. Yaghi, *Acc. Chem. Res.* **2008**, *41*, 1782.
[13] Z. Chen, S.-C. Xiang, T. Liao, Y. Yang, Y.-S. Chen, Y. Zhou, D. Zhao, B. Chen, *Cryst. Growth Des.* **2010**, *10*, 2775.
[14] T, Burchell, M. Rogers, *SAE Tech. Pap. Ser.* **2000**, 2000–01–2205.
[15] Elemental analysis calcd.(%) for UTSA-20 ($C_{48}H_{65}N_6O_{23.5}Cu_3$): C 44.60, H 5.07, N 6.50; found: C 44.36, H 4.69, N 6.39.
[16] T. Dueren, F. Millange, G. Ferey, K. S. Walton, R. Q. Snurr, *J. Phys. Chem. C* **2007**, *111*, 15350.
[17] a) S.-C. Xiang, W. Zhou, J. M. Gallegos, Y. Liu and B. Chen, *J. Am. Chem. Soc.* **2009**, *131*, 12415; b) S.-C. Xiang, W. Zhou, Z. Zhang, Y. Liu, B. Chen, *Angew. Chem.* **2010**, *122*, 4719; *Angew. Chem. Int. Ed.* **2010**, *49*, 4615.
[18] S.-I. Noro, S. Kitagawa, M. Kondo, K. Seki, *Angew. Chem.* **2000**, *112*, 2161; *Angew. Chem. Int. Ed.* **2000**, *39*, 2081.
[19] M. Kondo, M. Shimamura, S.-I. Noro, S. Minakoshi, A. Asami, K. Seki, S. Kitagawa, *Chem. Mater.* **2000**, *12*, 1288.
[20] M. Eddaoudi, J. Kim, N. Rosi, D. Vodak, J. Wachter, M. O'Keeffe, O. M. Yaghi, *Science* **2002**, *295*, 469.
[21] S. Ma, D. Sun, J. M. Simmons, C. D. Collier, D. Yuan, H.-C. Zhou, *J. Am. Chem. Soc.* **2008**, *130*, 1012.
[22] P. L. Llewellyn, S. Bourrelly, C. Serre, A. Vimont, M. Daturi, L. Hamon, G. D. Weireld, J.-S. Chang, D.-Y. Hong, Y. K. Hwang, S. H. Jhung, G. Ferey, *Langmuir* **2008**, *24*, 7245.
[23] X.-S. Wang, S. Ma, K. Rauch, J. M. Simmons, D. Yuan, X.-S. Wang, T. Yildirim, W. C. Cole, J. J. Lopez, A. De Meijere, H.-C. Zhou, *Chem. Mater.* **2008**, *20*, 3145.
[24] H. Wu, W. Zhou, T. Yildirim, *J. Phys. Chem. C* **2009**, *113*, 3029.
[25] H. Kim, D. G. Samsonenko, S. Das, G.-H. Kim, H.-S. Lee, D. N. Dybtsev, E. A. Berdonosova, K. Kim, *Chem. Asian J.* **2009**, *4*, 886.
[26] H. Wu, W. Zhou, T. Yildirim, *J. Am. Chem. Soc.* **2009**, *131*, 4995.
[27] H. Wu, J. M. Simmons, Y. Liu, C. M. Brown, X.-S. Wang, S. Ma, V. K. Peterson, P. D. Southon, C. J. Kepert, H.-C. Zhou, T. Yildirim, W. Zhou, *Chem. Eur. J.* **2010**, *16*, 5205.
[28] The claim of 220 $cm^3 cm^{-3}$ for PCN-14 was carried out at a lower temperature of 290 K. The expected volumetric methane storage capacity is expected to be lower at 300 K.
[29] A. R. Millward, O. M. Yaghi, *J. Am. Chem. Soc.* **2005**, *127*, 17998.
[30] W. Zhou, *Chem. Rec.* **2010**, *10*, 200.
[31] D. Frenkel, B. Smit, *Understanding Molecular Simulation: From Algorithms to Applications*, Academic Press, San Diego, **2002**.
[32] P. Giannozzi, S. Baroni et al., *J. Phys. Condens. Matter* **2009**, *21*, 395502 (see Supporting Information, Ref. [6]).
[33] V. Barone, M. Casarin, D. Forrer, M. Pavone, M. Sambi, A. Vittadini, *J. Comput. Chem.* **2009**, *30*, 934.
[34] A. C. Larson, R. B. Von Dreele, *General Structure Analysis System*, Report LAUR 86-748. Los Alamos National Laboratory, New Mexico (USA), **1994**.

